Electrical Percolation Behavior in Silver Nanowire–Polystyrene Composites: Simulation and Experiment

By *Sadie I. White, Rose M. Mutiso, Patrick M. Vora, David Jahnke, Sam Hsu, James M. Kikkawa, Ju Li, John E. Fischer,* and *Karen I. Winey**

The design and preparation of isotropic silver nanowire-polystyrene composites is described, in which the nanowires have finite *L/D* (< 35) and narrow *L/D* distribution. These model composites allow the *L/D* dependence of the electrical percolation threshold, ϕ_c, to be isolated for finite-*L/D* particles. Experimental ϕ_c values decrease with increasing *L/D*, as predicted qualitatively by analytical percolation models. However, quantitative agreement between experimental data and both soft-core and core–shell analytical models is not achieved, because both models are strictly accurate only in the infinite-*L/D* limit. To address this analytical limitation, a soft-core simulation method to calculate ϕ_c and network conductivity for cylinders with finite *L/D* are developed. Our simulated ϕ_c results agree strongly with our experimental data, suggesting i) that the infinite-aspect-ratio assumption cannot safely be made for experimental networks of particles with *L/D* < 35 and ii) in predicting ϕ_c, the soft-core model makes a less significant assumption than the infinite-*L/D* models do. The demonstrated capability of the simulations to predict ϕ_c in the finite-*L/D* regime will allow researchers to optimize the electrical properties of polymer nanocomposites of finite-*L/D* particles.

1. Introduction

Percolation concepts are used to describe an abrupt transition from one behavior to another, caused by the formation of long-range networks. They have been used to describe the concentration-dependent, insulator-to-conductor transition in composites of conductive fillers in insulating matrices, particularly polymer nanocomposites containing cylindrical fillers. These composites are technologically useful, because they combine the easy processability of the polymer matrix with the desirable electrical conductivity of the filler network. Such nanocomposites could find applications in static-discharge housing and packaging for electronics, EMI shielding, and light-weight, flexible conductors for electrodes, circuits, displays, and sensors.[1] As new functional nanoparticles of finite aspect ratio (*L/D*) become available, the ability to predict not only the electrical percolation threshold, ϕ_c, but also the properties (e.g., electrical conductivity) of networks above the percolation threshold, is increasingly important. Three-dimensional percolation behaviors of networks of cylinders have been extensively investigated by analytical,[2–4] simulation,[5–12] and experimental[7,12–21] methods; however, a systematic comparison of ϕ_c values obtained within the finite-*L/D* regime has not yet been performed. Such a comparison is critical for developing a robust predictive model of electrical percolation properties in networks of finite-*L/D* cylinders. Even a first-generation prognostic model, in which the electrical percolation threshold of an isotropic array of particles with known *L/D* could be predicted, would significantly increase the efficiency of nanocomposite design by decreasing the trial-and-error approach to predicting electrical properties.

The most commonly-used analytical approach for predicting ϕ_c for cylindrical fillers is the excluded volume model.[2,3,5–8,10,11] In this model, ϕ_c is inversely proportional to the "excluded volume" of the filler particles, which is the volume surrounding a particle into which the center of mass of a second, identical particle cannot enter without contacting it. The initial concept of the excluded volume model used soft-core particles, which were allowed to co-occupy space.[2,3,5,6,10] More recently, the model has been refined to account for core–shell particles, which can only overlap within a penetrable shell volume surrounding an impenetrable core.[7,8,11] In both the soft-core and core–shell cases, the model is analytically correct only in the $L/D \rightarrow \infty$ limit, so it is inappropriate for predicting percolation behaviors of particles with finite aspect ratios. However, because of the difficulties inherent in preparing conductive, cylindrical fillers with controlled aspect ratios, the aspect ratio regime in which the infinite-aspect-ratio assumption causes the model to fail has not yet been studied experimentally. In order to undertake the quantitative comparison of experimental and analytical percolation behaviors, one must first

[*] S. I. White, R. M. Mutiso, D. Jahnke, S. Hsu, J. Li, J. E. Fischer, K. I. Winey
Department of Materials Science and Engineering
University of Pennsylvania
Philadelphia, PA 19104 (USA)
E-mail: winey@seas.upenn.edu
P. M. Vora, J. M. Kikkawa
Department of Physics and Astronomy
University of Pennsylvania
Philadelphia, PA 19104 (USA)

DOI: 10.1002/adfm.201000451

select a model composite material that meets certain criteria. In addition to having finite aspect ratio and narrow aspect ratio distribution, the nanoparticles used in the study should be straight cylinders, and the conductivity of each particle should be roughly identical. Additionally, composites made using these model particles should have good particle dispersion. While numerous studies have been performed on the electrical percolation behaviors of carbon nanotube composites, carbon nanotubes are inappropriate as model materials for this type of finite-L/D percolation study, because they are highly flexible, contain a mixture of metallic and semiconducting morphologies, generally have poor aspect ratio and diameter control, and are notoriously difficult to disperse.

2. Results and Discussion

2.1. Measuring Experimental ϕ_c Values

We have prepared novel model composites of electrochemically-grown silver nanowires with mean aspect ratios of ~8, ~16, and ~31, which enable us to probe the extent of agreement between the experimental and analytical percolation thresholds for composites with relatively small aspect ratios. In addition to the obvious advantage of our synthetic control over their dimensions, silver nanowires are superior to carbon nanotubes in the context of our experiments because they are straight, they are sufficiently large that we can safely assume that they have minimal inter-particle variation in electrical conductivity, and they disperse easily into our experimental solvents and polymer. Example scanning electron microscopy (SEM) images of silver nanowires with $\langle L/D \rangle = 31.0 \pm 3.7$, 16.4 ± 1.5, and 8.23 ± 0.57 are shown in **Figure 1A–C**. At even our highest experimental aspect ratio, the nanowires appear to be straight, rigid objects. Figure 1D shows a nanocomposite fracture surface, representative of the high degree of nanowire dispersion that is typical of our preparation method.

To determine the volume percolation thresholds (ϕ_c values) for composites with different aspect ratio wires, the conductivity of the samples was calculated by fitting their current–voltage (I–V) characteristics with the "fluctuation-assisted tunneling" model developed by Kaiser and Park.[22] This model is based on the work of Sheng,[23] and accounts for field enhancement of tunneling probabilities between conducting regions separated by insulating barriers. The model describes the

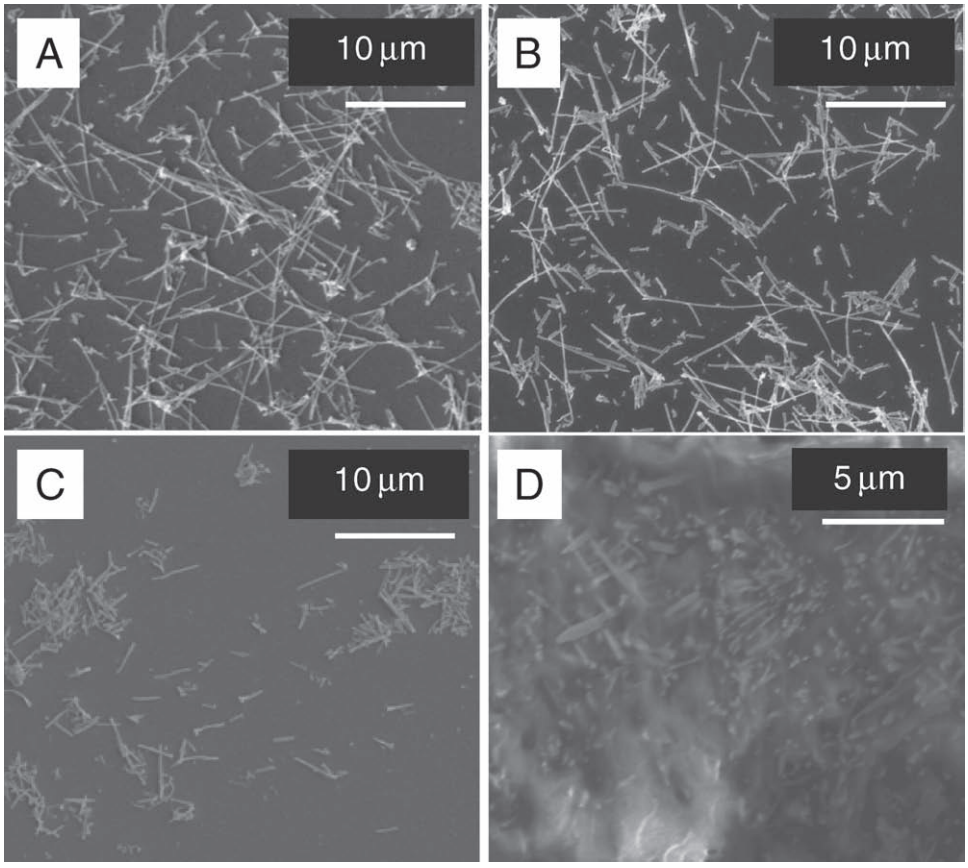

Figure 1. SEM images for silver nanowires with diameters of ~200 nm and average aspect ratios of A) 31.0 ± 3.7, B) 16.4 ± 1.5, and C) 8.23 ± 0.57. An SEM image of a cross section of a freeze-fractured composite (wire dimensions of $\langle L/D \rangle \approx 16$ and $\phi = 0.061$) is shown in (D). The good dispersion observed in this composite was also observed in composites with all $\langle L/D \rangle$ and all ϕ.

voltage-dependent transition between macroscopic low-field and high-field (i.e., "saturated") conductance states, G_0 and G_h, respectively:

$$I = \frac{V G_0 \exp\left(\frac{V}{V_0}\right)}{1 + \frac{G_0}{G_h}\left[\exp\left(\frac{V}{V_0}\right) - 1\right]}. \quad (1)$$

In Equation 1, V_0 is related to the barrier height separating the conductive regions, although the specific shape of the barrier is not captured in the model. Equation 1 has been applied to a number of different systems, including single-walled carbon nanotubes,[24] V_2O_5 nanowires,[25] granular Sr_2FeMoO_6,[26] and polyacetylene nanofibers.[27,28] Representative fits of our experimental data to this model are shown in **Figure 2**. The G_h values were taken as the representative conductance values for the nanowire composite networks, and were used to calculate the conductivity, σ, of each sample by: $\sigma = G_h/(l_s/(w_s h_s))$, where l_s, w_s, and h_s are the length, width, and height of the sample, respectively.

The composite electrical conductivity is plotted as a function of filler volume fraction, ϕ, for all three experimental aspect ratios in **Figure 3A–C**. For each aspect ratio, the nanocomposite conductivities are plotted with the conductivity of a solvent-cast mat of nanowires prepared by each method (unsonicated or sonicated for 12 or 24 h in methanol). The mats were prepared by solvent-casting a ~2.5 mg suspension of purified nanowires in ~2 mL methanol into a rectangular Teflon pan to create a mat with dimensions of ~1 cm × 1 cm. The resistances of the mats were calculated using four-probe electrical *I–V* measurements. After the measurements were taken, the mass of the wires composing each mat was measured, and the effective thickness of each mat was calculated using the density of silver (10.6 g cm^{-3}), and assuming the mats are fully dense. This thickness value was used to calculate the conductivity of each mat, using

$$\sigma_{mat} = \frac{1}{R_m}\left(\frac{l_m}{w_m t_{eff}}\right), \quad (2)$$

in which R_m is the measured resistance of each mat, l_m is the mat length, w_m is the mat width, and t_{eff} is the effective mat thickness. This procedure yields a value of the mat conductivity from the measured resistance that is based on the actual nanowire volume, not exterior dimensions. Each mat, consisting of ~1×10^9 nanowires, has a conductivity significantly lower than the conductivity of pure silver (~6×10^5 S cm^{-1}), likely because the conductivity of the mats is reduced by the contact resistances of the numerous wire-wire contacts present in each mat. For both the $\langle L/D \rangle \approx 8$ and $\langle L/D \rangle \approx 31$ composites, the maximum conductivity of the composites is below the conductivity of the mats. However, the maximum conductivity of the $\langle L/D \rangle \approx 16$ composites is on the order of the conductivity of its corresponding mat.

In the composite conductivity data in Figure 3, the electrical percolation transition for each $\langle L/D \rangle$ is observed as a dramatic increase in the electrical conductivity as ϕ increases above the critical volume fraction, ϕ_c, and is described by

$$\sigma \approx \left(\frac{\phi - \phi_c}{\phi_c}\right)^{\alpha}, \quad (3)$$

close to the percolation transition. The experimental fits to Equation 3 that were used to determine experimental ϕ_c values are shown in Figure 3D–F. As expected, ϕ_c decreases with increasing filler aspect ratio; $\phi_c = 0.083$ for $\langle L/D \rangle \approx 8$, $\phi_c = 0.059$ for $\langle L/D \rangle \approx 16$, and $\phi_c = 0.023$ for $\langle L/D \rangle \approx 31$. The data do not tightly constrain the exponent α. Nevertheless, we do not observe the theoretically-predicted "universal exponent" of 2, expected for three-dimensional percolation. This result is not surprising, as non-universal exponents can arise when tunneling is a dominant charge transport mechanism, as is the case here.[29]

2.2. Simulating ϕ_c Values

Because excluded volume models for cylinders are only appropriate for fillers with effectively infinite aspect ratios, we have developed a simulation to determine the isotropic percolation thresholds for composites containing finite-aspect-ratio cylindrical fillers. We have previously used this simulation to study the effects of uniaxial cylinder alignment on electrical percolation.[9] In the simulation, a random configuration of straight,

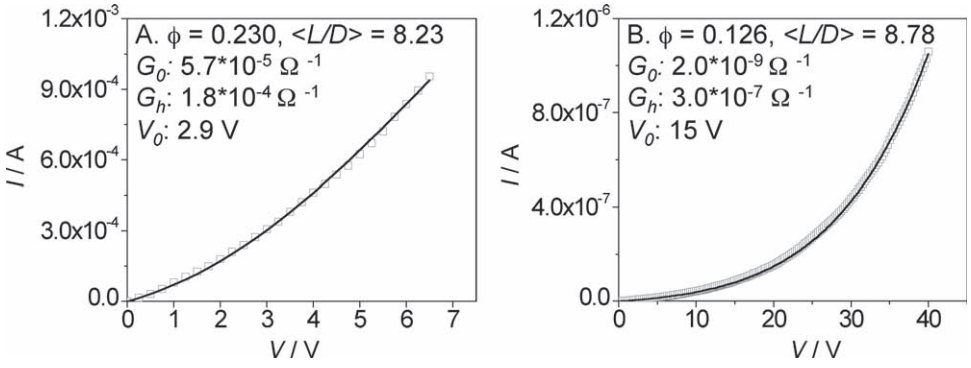

Figure 2. Sample fits of *I–V* data for two composites with $\langle L/D \rangle \approx 8$ with the fluctuation-assisted tunneling (FAT) model developed by Kaiser and Park, Equation 1.[22] For both samples, the points (□) are experimental data, while the solid lines are the best fit results of the fluctuation-assisted tunneling model. The saturation-conductance (G_h) values were used to calculate the conductivity of each sample.

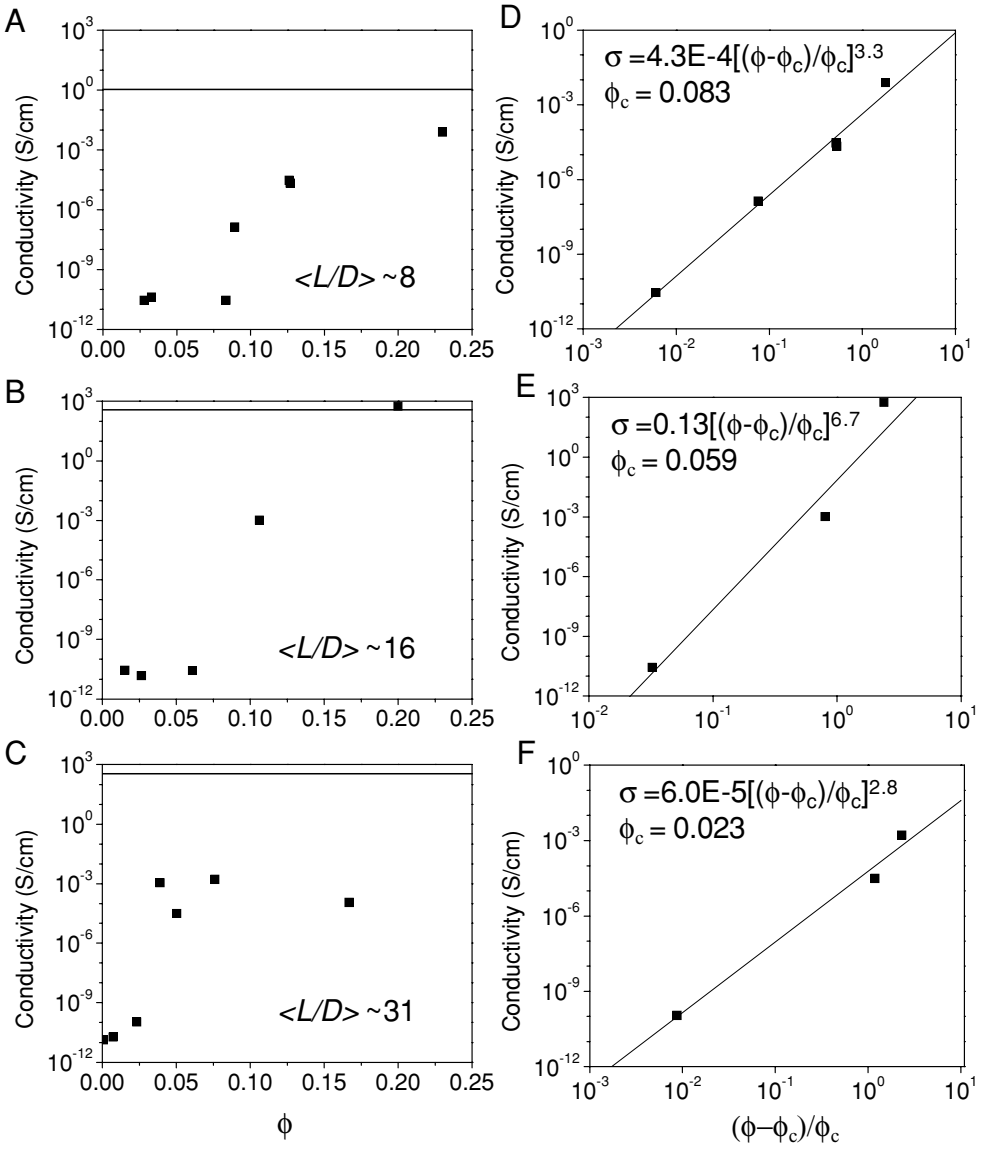

Figure 3. Electrical conductivity (■) vs. ϕ for composites with A) $<L/D> \approx 8$, B) 16, and C) 31. Conductivities were calculated from the fluctuation-assisted tunneling model (Equation 1). One standard deviation in ϕ was determined from TGA to be ± 0.002 (smaller than the plot symbols). The solid lines in (A–C) represent the conductivity of a mat of nanowires with each $<L/D>$. D–F) show the calculation of ϕ_c for $<L/D> \approx 8$, 16, and 31, respectively.

cylindrical rods of prescribed aspect ratio and orientation distribution is generated in a large supercell. The supercell has been divided into tiling cubic sub-blocks, whose length is greater than the rod size, and rods which fall into each sub-block are registered. Aided by the sub-block data structures, the possible neighbors of each rod are determined (they cannot fall outside of the surrounding 26 sub-blocks and the central sub-block), with computational complexity that scales linearly with the total number of rods. Then, the shortest distance between two possible neighboring rods is calculated using a close-formed formula, from which one can determine whether they are actually in contact. A clustering analysis is then carried out to decompose the rod configuration into: a) clusters of contacting rods that simultaneously touch the top and bottom surfaces of the supercell, and b) clusters that do not. The total conductance is just the sum of the individual cluster conductances in (a), and the (b) clusters are simply ignored because they do not form a percolating path. For each cluster in (a), one assumes every rod i has a uniform voltage V_i (no internal resistance) that is an unknown variable, except for those rods which touches the top ($V_i = 1$) or the bottom ($V_i = 0$). A system of linear equations $Ax = b$ is then established for each cluster, assuming that all the electrical resistance results from contact resistances between neighboring rods, and the sum of electrical currents that flow into any rod (that is not touching the top or bottom surface) must be

zero. This system of linear equations is solved using the preconditioned conjugate gradient iterative (KSPCG) method[30] as implemented in the Portable, Extensible Toolkit for Scientific Computation (PETSc) package, where the incomplete LU factorization preconditioner (PCILU) is used, to obtain the cluster conductance. This whole procedure is then repeated, and a large number of configurations are generated, to obtain the ensemble-averaged conductance. The resulting simulated conductivities are plotted vs. ϕ for representative values of L/D in **Figure 4**. ϕ_c values for each of the simulated aspect ratios were determined by fitting the simulation data to Equation 3. These fits are shown in the Supplemental Information, Figure S2. As in the experimental data, the simulated data show a decrease in ϕ_c with increasing L/D.

2.3. Comparison to Analytical ϕ_c Values

We first compare our experimental and simulation ϕ_c values to those obtained from the soft-core excluded volume model.[2,3,5,6,10] The excluded volume of a single soft-core, penetrable, cylinder in an isotropic array of identical cylinders is

$$V_{ex,s-c} = 8\pi L R^2 + \pi L^2 R, \tag{4}$$

where L is the length of the cylinder, and R is its radius. The excluded volume of a particle (i.e., the volume around a cylinder into which the center of mass of a second, identical particle cannot enter without coming into contact with the first) is related to the critical number of particles required for geometrical percolation of soft-core cylinders ($N_{c,\,s-c}$) by

$$N_{c,s-c} \cong \frac{V}{V_{ex,s-c}}, \tag{5}$$

where V is the total sample volume. In the slender-rod limit (i.e., as $L/D \to \infty$), this relation becomes a true equality. Using the slender-rod assumption for isotropic, soft-core cylinders, ϕ_c is given by

$$\phi_{c,s-c} = \frac{N_{c,s-c}(\pi R^2 L)}{V} = \frac{V(\pi R^2 L)}{V \times V_{ex,s-c}} = \frac{(\pi R^2 L)}{8\pi R^2 L + \pi L^2 R}. \tag{6}$$

For particles with finite aspect ratio, the slender-rod assumption can introduce significant error. The significance of the infinite-aspect-ratio assumption can be seen with a simple calculation. For spherical fillers ($L = D$), the ϕ_c value calculated from Equation 6 is 0.10, which is significantly less than the value of 0.35 obtained from percolation models of interpenetrable spherical particles.[8] Therefore, it is reasonable to expect that there is some finite L/D value at which this excluded volume model for cylinders breaks down.

The ϕ_c values obtained from our experiments (Figure 3) and simulations (Figure 4) are plotted vs. cylinder aspect ratio, along with the solutions obtained from the soft-core, slender-rod, analytical model in **Figure 5A**. The figure makes two primary points. First, the soft-core excluded volume model predicts lower ϕ_c values than both the simulation and experimental approaches, for all L/D. While there is reasonable agreement between the simulation and model results at $L/D > 60$, the discrepancy is more pronounced as L/D decreases. Additionally, there is reasonable agreement between the simulation and experimental ϕ_c values. This suggests that the simulation model (containing interpenetrable, finite-L/D cylinders) is more accurate in describing experimental systems containing finite aspect ratio rods than the soft-core analytical model (containing interpenetrable, infinite-L/D cylinders).

The core–shell excluded volume model operates under the same principles (and infinite L/D assumption) as the soft-core model, but defines an excluded volume that allows the particles to overlap only within a shell of defined thickness. Berhan and Sastry[7] provide a modified expression for ϕ_c:

$$\phi_{c,c-s} = \frac{(\pi R^2 L)}{8\pi r^2 L(1-t^2) + \pi r L^2(1-t)}, \tag{7}$$

where R is the radius of the impenetrable core, r is the outer shell radius (i.e., the radius of the impenetrable core plus the penetrable shell), and $t = R/r$. In the soft-core limit, $t = 0$, and in the hard-core limit, $t = 1$. Figure 5B shows a comparison of the experimental and simulation ϕ_c values with the core–shell model, using t values of 0.9 and 0.8 (Equation 7). Given an average silver nanowire radius of 100 nm, these values of t corresponded to penetrable shell diameters of 11 nm and 25 nm, respectively, which are reasonable upper limits to inter-particle tunneling. Although the core–shell analytical model contains a more physically reasonable assumption (i.e., that the particles are not allowed to overlap in space), the core–shell model curves with $t = 0.8$, and $t = 0.9$ both overestimate experimental ϕ_c values, and again, the closest agreement is obtained between the simulation and experimental data.

By comparing the ϕ_c values obtained from our experimental composites (which contain finite-aspect-ratio, polydisperse, impenetrable particles), our simulations (which contain finite-aspect-ratio, monodisperse, penetrable particles), and the soft-core

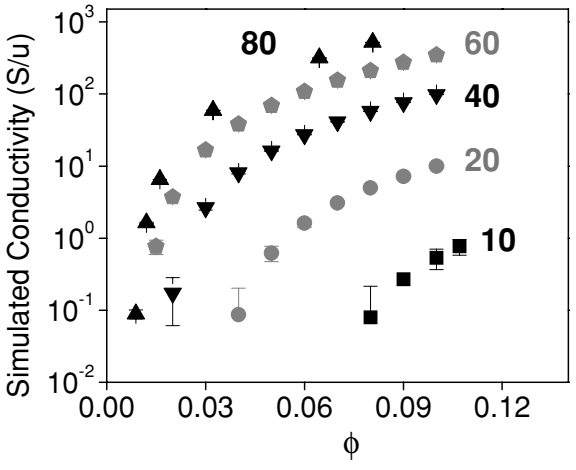

Figure 4. Calculated electrical conductivity vs. ϕ for simulated composites with L/D 80, 60, 40, 20, and 10. Error bars represent ± one standard deviation in conductivity, and are often smaller than the plot symbols. Aspect ratios are listed next to the data sets.

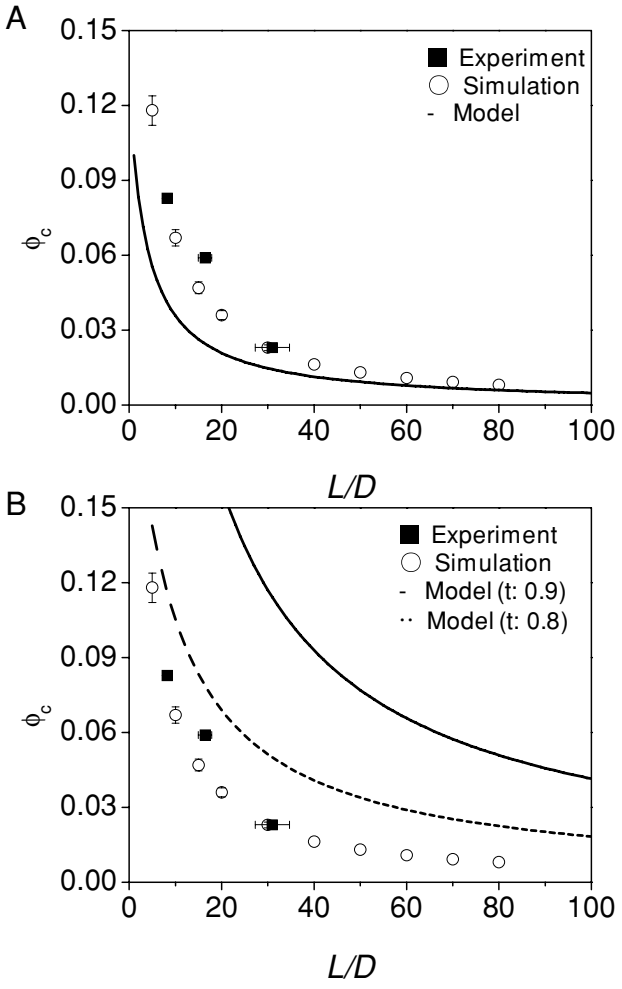

Figure 5. A) ϕ_c vs. L/D for experimental (■) and simulated (○) composites, as well as the soft-core analytical model (solid line). Error bars are added to the simulation data by taking into account the minor finite size effects in our simulation method to determine ϕ_c, error < + 5%; see description in the Supplemental Information. At $L/D > 20$, this effect leads to error bars that are smaller than the symbol size. Error bars on the experimental data show standard deviations in silver nanowire $<L/D>$. B) ϕ_c vs. L/D for experimental (■) and simulated (○) composites, as well as the core–shell analytical model with $t = 0.9$ (solid line) and $t = 0.8$ (dashed line).

and core–shell excluded volume models (both of which assume infinite-aspect-ratio, monodisperse particles), we can isolate the individual significance of the assumptions made in the analytical models and simulations. All of the non-experimental approaches that we address in this paper assume the existence of perfectly monodisperse cylinders. Given the magnitude of the discrepancies in ϕ_c between the experimental and analytical models, relative to the standard deviation in L/D of our silver nanowires (<12%), it is reasonable to conclude that the assumption of monodispersity is probably insignificant. This leaves two factors in which the experimental data deviate significantly from the non-experimental approaches; the experimental composites contain fillers i) with finite aspect ratio and ii) that do not co-occupy space. The effects of the finite-aspect ratio assumption can be most clearly observed by comparing ϕ_c values from experiments, simulations, and the soft-core excluded volume model (Figure 5A). While both the simulation and the model allow the filler particles to co-occupy space (which is an assumption not borne out in the experimental samples), only the simulations contain finite-aspect-ratio fillers (which is also true of the experimental samples). As is clear in Figure 5A, the experimental ϕ_c values agree better with the simulation ϕ_c values than the soft-core ϕ_c data at $L/D < 60$. The simulations more closely approximate experimental ϕ_c by removing the assumption of infinite filler aspect ratio. Thus, we conclude that at $L/D < 60$, finite aspect ratio considerations must be incorporated into percolation models of cylindrical rods to have accurate predictions of ϕ_c.

Although Figure 5A demonstrates that the assumption of penetrable versus impenetrable particles is secondary to the paramount issue of finite aspect ratios, it is instructive to compare the soft-core and core–shell models. From Figure 5A and B, it is clear that the soft-core assumption leads to an underestimation of ϕ_c, compared to both experimental and core–shell ϕ_c values. This is reasonable because there is increased statistical likelihood of two cylinders coming into contact if they are allowed to overlap completely, instead of through a thin shell region. Therefore, the soft-core assumption results in the formation of more cylinder–cylinder contacts than are physically possible in our experimental systems, or than are permitted in the core–shell model. It is also clear that there is significant dependence of the quality of the fit on t. Finally, because the error from the infinite-aspect-ratio assumption is still present in the core–shell model, it should not be necessarily assumed that increased agreement obtained by decreasing t negates the error contributed by the infinite-aspect-ratio assumption. Recall that $t = 0.8$ corresponds to a shell thickness of 25 nm in our silver nanowire-polystyrene composites, which is already larger than expected tunneling distances in an insulating, glassy polymer. An even smaller t value seems physically unreasonable. Thus, the impenetrable core condition in the core–shell analytical model is secondary, while the finite-aspect-ratio condition in the simulations is paramount for obtaining good agreement with experimental data.

3. Conclusions

We describe comparisons of electrical percolation thresholds, ϕ_c, for networks of finite-L/D cylinders obtained from experimental composites, simulations, and analytical models. The goal of our investigations was to identify the significant elements comprising the best predictors of experimental ϕ_c values, and develop a predictive approach that would guide researchers in the design of electrically-functional nanocomposites. Our experimental ϕ_c values agree more closely with our simulations (which contain finite-L/D, soft-core cylinders) than with both soft-core and core–shell analytical models (both of which assume infinite-L/D cylinders). This suggests that accounting for finite L/D is more critical in predicting experimental ϕ_c than expressly preventing non-physical particle-particle overlap. We propose that our existing simulation method, despite containing the non-physical assumption that the particles can co-occupy space, is a powerful first-generation predictor of experimental

ϕ_c in the finite-L/D regime. Effective prediction of ϕ_c allows researchers to design composites that optimize electrical properties of the filler (by generating networks with $\phi > \phi_c$), while minimizing total filler volume fraction, which reduces total cost and improves nanocomposite processability. This may prove particularly effective for the design of fuel cell electrodes, which are often made with conductive nanocomposites, or simply mats of conductive particles.

We are in the process of modifying our soft-core simulation method to address more complex arrays of particles, including impenetrable cylinders, cylinders with L/D polydispersity and bimodal L/D distributions, interparticle attractions, and inhomogeneous particle distributions. Each of these modifications is being considered to make the simulation method more universally applicable to percolation behaviors for a variety of cylindrical particles. We are also working to incorporate more physically appropriate values and variations in interparticle contact resistance, which may improve the predictions of network conductivity in the simulations. By inserting measured interparticle contact resistance into the simulations, we could use our simulation methodology to predict conductivity values for networks of different types of particles, enhancing its predictive capabilities beyond simple percolation threshold predictions.

4. Experimental Section

Silver Nanowire Synthesis: Silver nanowires were prepared by electroplating into commercially-available, porous Al_2O_3 membranes with ~200 nm diameter pores (42 mm diameter, Whatman Anodisc, 6809-5022). The membranes were coated on one side with Ga/In eutectic, then the coated side was attached to a copper electrode. The electrode was coated with electrically-insulated waterproof varnish, such that only the portion touching the membrane was exposed. The plating was performed in the dark in a bath of 45 g L^{-1} $AgNO_3$ and 45 g L^{-1} H_3BO_3 in Millipore deionized H_2O at 10 V AC current for 2 min. This procedure was repeated with a fresh membrane to obtain the desired mass of nanowires (~2.5 mg per membrane). The Ga/In was removed, then the membranes were dissolved overnight in a stirred, room temperature 1.0 M NaOH solution in Millipore deionized H_2O (5 mL per membrane). According to the Pourbaix diagram for silver,[31] processing at this pH yields oxide-free nanowire surfaces. The wires were pelleted from the solution by centrifuging at 2100 rcf for 5 min, then washed sequentially with Millipore deionized H_2O and methanol, and finally suspended in toluene at a concentration of ~ 10 mg mL^{-1}. A sample of the wire suspension for each composite was removed deposited onto a silicon wafer to be imaged in an FEI Strata DB235 SEM. A total of 100 measurements of wire length and wire diameter were taken from the SEM images using ImageJ analysis software. The as-prepared nanowires had a typical diameter of ~200 nm and a typical length of ~6 μm ($<L/D> \approx 31$). To obtain wires with $<L/D> \approx 16$ and $<L/D> \approx 8$, suspensions of nanowires in methanol were sonicated using a bath sonicator for 12 or 24 h, respectively, then subjected to SEM and image analysis as previously described. For both the sonicated and unsonicated samples, the average diameter of the wires was statistically identical (~200 nm); the aspect ratio changed only because the wires became shorter during sonication.

Nanowire Composite Preparation: Nanocomposites were prepared by adding the appropriate amount of polystyrene ($M_w \approx$ 190k, Scientific Polymer Products, #846) to the nanowire suspension in toluene and stirring vigorously at room temperature for 24 h to ensure complete polymer dissolution. The suspension was then precipitated by adding it to a large excess of vigorously-stirring methanol. This produced a fine gray powder, which was then filtered off from the colorless filtrate and vacuum-dried at 125 °C for 24 h. This method produced a consistently good nanowire dispersion, which was checked by freeze-fracturing composite samples and imaging the fracture surfaces with SEM. The mass fraction of nanowires in a given composite was determined by thermogravimetric analysis (TGA; TA Instruments SDT 2960), using a 20 °C min^{-1} temperature sweep to 400 °C, then an isothermal hold for 180 min. The residual mass of the nanowires was then converted to volume fraction, ϕ. TGA was repeated in triplicate for both a high- and low-ϕ composites, and the resulting variation in the calculated ϕ for each composite was 0.002. The nanocomposite powders were hot-pressed into a rectangular die at 150 °C, using a Carver Model C hot press, to create bars of dimensions ~1 cm × ~0.2 cm × ~0.2 cm (~75 mg). To check that the hot-pressing procedure did not induce any significant alignment to the samples, small-angle X-ray scattering was performed on the sample along the measurement direction. A 2D scattering pattern is shown in the Supporting Information, Figure S1 A, and shows isotropic scattering. A fit of the I vs. q data is presented in the Supporting Information, Figure S1 B, and shows an $I \sim q^{-4}$ dependence, which is consistent with cylinder form factor scattering. This suggests that the hot pressing technique did not introduce any significant alignment in the nanowire composites.

Electrical Characterization: The ends of the hot-pressed composite bars were coated with silver paint and subjected to 2-probe I–V measurements at room temperature under ambient conditions, using a Keithley 237 source-measurement unit with a Labview software interface. In all cases, the measurements were made by sourcing voltage and measuring current. The current compliance was set to 10^{-3} A. The voltage increment for these scans was 0.25 V, the sweep rate was ~1.4 s per increment, and the readings were recorded with a 32 reading filter. The conductivity of the sample containing nanowires with $<L/D> \approx 16$ and $\phi = 0.200$ was measured with a 4-probe configuration, using the same instrumentation as the 2-probe measurements.

Supporting Information

Supporting Information is available online from Wiley InterScience or from the author.

Acknowledgements

We acknowledge the Penn Regional Nanotechnology Facility. S.I.W. acknowledges financial support from the GRFP at the National Science Foundation. K.I.W., J.M.K, J.L., and P.M.V. acknowledge financial support from the Materials Research Science and Engineering Center, National Science Foundation (Grant No. DMR-05-20020).

Received: March 9, 2010
Revised: April 20, 2010
Published online: July 1, 2010

[1] D. D. L. Chung, *J. Mater. Sci.* **2004**, *39*, 2645.
[2] A. L. R. Bug, S. A. Safran, I. Webman, *Phys. Rev. Lett.* **1985**, *54*, 1412.
[3] A. L. R. Bug, S. A. Safran, I. Webman, *Phys. Rev. B* **1986**, *33*, 4716.
[4] S. Kirkpatrick, *Rev. Mod. Phys.* **1973**, *45*, 574.
[5] I. Balberg, C. H. Anderson, S. Alexander, N. Wagner, *Phys. Rev. B* **1984**, *30*, 3933.
[6] I. Balberg, N. Binenbaum, N. Wagner, *Phys. Rev. Lett.* **1984**, *52*, 1465.
[7] L. Berhan, A. M. Sastry, *Phys. Rev. E* **2007**, *75*, 041120, and references therein.
[8] A. L. R. Bug, S. A. Safran, G. A. Grest, I. Webman, *Phys. Rev. Lett.* **1985**, *55*, 1896.
[9] S. I. White, B. DiDonna, M. Mu, T. C. Lubensky, K. I. Winey, *Phys. Rev. B* **2009**, *79*, 024301.

[10] Z. Néda, R. Florian, Y. Brechet, *Phys. Rev. E* **1999**, *59*, 3717.
[11] I. Balberg, N. Binenbaum, *Phys. Rev. A* **1987**, *35*, 5174.
[12] N. Hu, Z. Masuda, C. Yan, G. Yamamoto, H. Fukunaga, T. Hashida, *Nanotechnology* **2008**, *19*, 215701.
[13] F. Du, R. C. Scogna, W. Zhou, S. Brand, J. E. Fischer, K. I. Winey, *Macromolecules* **2004**, *37*, 9048.
[14] M. B. Bryning, M. F. Islam, J. M. Kikkawa, A. G. Yodh, *Adv. Mater.* **2005**, *17*, 1186.
[15] J. Sandler, S. P. Shaffer, T. Prasse, W. Baunhofer, K. Schulte, A. H. Windle, *Polymer* **1999**, *40*, 5967.
[16] F. Du, J. E. Fischer, K. I. Winey, *J. Polym. Sci. Part B: Polym. Phys.* **2003**, *41*, 3333.
[17] S. Stankovich, D. A. Dikin, G. H. B. Dommett, K. M. Kohlhaas, E. J. Zimney, E. A. Stach, R. D. Piner, S-B. T. Nguyen, R. S. Ruoff, *Nature* **2006**, *442*, 282.
[18] J. K. W. Sandler, J. E. Kirk, I. A. Kinloch, M. S. P. Shaffer, A. H. Windler, *Polymer* **2003**, *44*, 5893.
[19] B. E. Kilbride, J. N. Coleman, J. Fraysse, P. Fournet, M. Cadek, A. Drury, S. Hutzler, S. Roth, W. J. Blau, *J. Appl. Phys.* **2002**, *92*, 4024.
[20] I. Balberg, D. Azulay, D. Toker, O. Millo, *Int. J. Mod. Phys. B* **2004**, *18*, 2091.
[21] W. Bauhofer, J. Z. Kovacs, *Comp. Sci. Technol.* **2009**, *69*, 1486.
[22] A. B. Kaiser, Y. W. Park, *Synthetic Metals* **2005**, *152*, 181.
[23] P. Sheng, *Phys. Rev. B* **1980**, *21*, 2180.
[24] S. W. Lee, D. S. Lee, H. Y. Yu, E. E. B. Campbell, Y. W. Park, *Appl. Phys. A* **2004**, *78*, 283.
[25] G. T. Kim, J. Muster, V. Krstic, J. G. Park, Y. W. Park, S. Roth, M. Burghard, *Appl. Phys. Lett.* **2000**, *76*, 1875.
[26] B. Fisher, K. B. Chashka, L. Patlagan, G. M. Reisner, *Phys. Rev. B* **2003**, *68*, 134420.
[27] J. G. Park, B. Kim, S. H. Lee, A. B. Kaiser, S. Roth, Y. W. Park, *Synth. Met.* **2003**, *135–136*, 299.
[28] J. G. Park, G. T. Kim, V. Krstic, S. H. Lee, B. Kim, S. Roth, M. Burghard, Y. W. Park, *Synth. Met.* **2001**, *119*, 469.
[29] N. Johner, C. Grimaldi, I. Balberg, P. Ryser, *Phys. Rev. B.* **2008**, *77*, 174204.
[30] M. R. Hestenes, E. Stiefel, E., *J. Res. Natl. Bur. Stand.* **1952**, *49*, 409.
[31] D. A. Jones, *Principles and Prevention of Corrosion*, Prentice Hall, New Jersey **1996**.